Simple nanosilver composite for photocatalytic inactivation of *Salmonella typhimurium*

Xiao-Lan Wei[1] ✉, *Yuan-Yuan Qi*[2]

[1]*Chongqing Key Laboratory of Catalysis and Functional Organic Molecule, College of Environment and Resources, Chongqing Technology and Business University, Chongqing 400067, People's Republic of China*
[2]*College of Computer Science and Information Engineering, Chongqing Technology and Business University, Chongqing 400067, People's Republic of China*
✉ *E-mail: weishine@ctbu.edu.cn*

Published in Micro & Nano Letters; Received on 1st September 2016; Revised on 27th December 2016; Accepted on 5th January 2017

Photocatalytic killing of *Salmonella*, one of the most dangerous foodborne pathogens is developed using silver nanoparticles (AgNPs)-decorated silver chloride grains which is one of the simplest nanosilver composites. This nanosilver composite was synthesised using a precipitation–reduction method and was found to have a strong and broad absorption band of light in the range from visible to near infrared. Inactivation of *Salmonella typhimurium* using the nanocomposite was significantly enhanced by the irradiation of the visible light, which is due to the surface plasmon resonance of the AgNPs. Plasmonic electrons of the nanoparticle could be transferred to the oxygen molecules in the bacterial solution to produce reactive oxygen species (ROSs), while the corresponding holes could oxidise chloride ions of the AgCl grain to form chlorine atoms. Both ROSs and chlorine atoms degrade biomolecules of the bacterial cell, which was revealed by the Fourier transform infrared spectroscopy of the bacterial cells with the help of chemometric analysis.

1. Introduction: *Salmonella* is recognised as one of the major causes of foodborne diseases in humans worldwide, sometimes accounting for the highest morbidity and mortality rates among foodborne pathogens. Despite the fact that *Salmonella* infections result in high economic and social costs, the efficient control of this microorganism remains a hard challenge in in food production systems [1]. In the past decades, various novel technologies, such as nanostructure-based disinfection and photocatalytic sterilisation, have emerged with great potential to inactivate *Salmonella* and other foodborne pathogens [2].

Silver and its compounds behave strong bactericidal activities and low toxicities to human cells and have been used as antimicrobials to fight infections and prevent spoilage for centuries [3]. Recently, silver in the form of nanoparticles (AgNPs) was also known to present strong biocidal effects on a broad spectrum of microorganisms [4, 5], including multidrug resistant *Salmonella typhimurium* (*S. typhimurium*) [6]. It is generally accepted that AgNPs and silver ions released from the nanomaterial are able to damage the membrane structures, bind the proteins, and interact with the DNA molecules of the target cell [7–9].

Besides being employed alone, AgNPs were also coupled with a semiconductor (such as titania) to enhance the activity of photocatalytic disinfection [10]. The photocatalyst, usually used for the oxidising degradation of organics, adsorbs photons and gives pairs of electron and hole, which react to give reactive oxygen species (ROSs) such as $\cdot O_2^-$ and ·OH [11]. Modification of the photocatalyst with AgNPs takes advantages of not only the electron trapping effect to decrease the electron–hole recombination, but also the local surface plasmon resonance (SPR) to increase the visible light utilisation [12]. Nowadays, a variety of nanosilver composites which were synthesised by various chemical or biological methods have been exploited for the photocatalytic killing of a wide range of microorganisms [13–16], opening up a new green way to combat bacterial pathogens.

However, no data concerning the photocatalytic inactivation of *Salmonella* are available to date, including the simplest nanosilver composite, AgNPs-decorated silver chloride grain (AgNPs@AgCl). The AgNPs@AgCl composite was constructed by forming AgNPs on the particle of AgCl, in which AgNPs act as both a light absorbent and a photocatalyst. It is different to most of the nanosilver-modified photocatalysts, and was proven to be highly stable and efficient for destroying organic dyes [17]. The aims of this Letter were to test the antimicrobial effectiveness of the simplest nanosilver composite under visible light illumination against *Salmonella typhimurium*. In addition, the Fourier transform infrared spectroscopy (FTIR) combined with chemometric analysis has been used for the study of the antimicrobial mechanism at a molecular level, dissecting the structure changes in *S. typhimurium* that occurs in the photocatalytic inactivation using AgNPs@AgCl.

2. Materials and methods: All chemicals used in this work were of analytical grade and used as-received without any further purification. The *S. typhimurium* strain CMCC50115 used in this Letter was obtained from National Center for Medical Culture Collections (CMCC, China).

The AgNPs@AgCl nanocomposite was prepared by a precipitation–reduction method. Typically, a 10-ml solution of NaCl (1 mmol) was dropwise added into a 30-ml fresh solution dissolving $AgNO_3$ (1 mmol) and polyvinyl pyrrolidone (PVP, 0.25 g) with vigorous stirring, forming a milky solution dispersing AgCl particles. Then a 2-ml 1 M Tris solution which acted as a reducing agent was added into the above solution. Subsequently, the obtained AgCl emulsion was irradiated by a UV lamp (TUV 8 W, 254 nm, Philips, the Netherland) for 15 min to produce the Ag@AgCl nanocomposite. Finally, the product was collected by centrifugation, washed with deionised water three times, and dried at 60°C overnight.

The morphology of the samples was characterised by field emission scanning electron microscopy (FESEM) on a JSM-7800F microscope (JEOL, Japan) at 10 kV. The crystal phase was determined by X-ray diffraction (XRD) measurements using a XRD-6000 (Shimadzu, Japan) with Cu Kα radiation. The UV−vis absorption spectra were measured with a UV-2450 spectrometer (Shimadzu, Japan).

S. typhimurium was used as the target bacterium in this Letter, which was grown in the Luria-Bertani (LB) broth at 37°C with shaking for 12 h. The bacterial sample and the Ag@AgCl composite

were suspended in the LB broth and mixed by a magnetic stirrer, and the initial cell density was adjusted to the optical density at 600 nm (OD_{600}) reached 0.20, corresponding to a bacterial concentration of $\sim 1.0 \times 10^8$ CFU/ml. Simultaneously, the mixture was irradiated by an LED lamp with a peak wavelength of 590 nm (Luxeon LXHL-LL3C, Philips Lumileds Lighting Co., USA) with a UV cutoff filter ($\lambda < 400$ nm). The irradiation intensity on the sample was determined to be 18.3 mW/cm^2 by a light meter (LI-COR, Lincoln, Nebraska, USA). Light controls (light alone without photocatalyst) and dark controls (AgNPs@AgCl alone without light) were carried out for each set of experiment. All experimental controls and treatments were performed in triplicate. The concentration of the AgNPs@AgCl composite (mg/l) was adjusted to 0, 10, 20, 50, 100, respectively, the solution pH was 6.75 and the temperature was 30°C, unless stated.

A growth assay was carried out to evaluate the antibacterial activity of the AgNPs@AgCl composite. One ml of the reaction solution was sampled at different time intervals (h), including 0, 0.5, 1.0, 2.0, 4.0, and 6.0. The OD_{600} was measured for all samples by an UV-2450 spectrometer to obtain the growth curve of *S. typhimurium*. Considering that the AgNPs@AgCl particles in the medium would greatly influence the optical density of the solution, the OD_{600} of LB medium containing the AgNPs@AgCl of the same concentration without *S. typhimurium* was deducted to obtain the actual OD_{600} of the bacterial sample.

FTIR spectroscopy was used to assess molecular changes in *S. typhimurium* cells after the photocatalytic inactivation. Five millilitres of the bacterial sample cultured in LB broth was washed with saline (0.90% NaCl), through centrifuging the bacteria at 4000 rpm for 5 min, removing the supernatant and re-suspending the cell pellet in 5.0 ml of saline. This saline washing was carried out five times to remove the LB broth completely. Then, a 100-µl saline solution of the bacteria was dropped onto a silicon slice and dried 30 min at 37°C for the FTIR measurement. The FTIR spectra were acquired from IR Prestige-21 (Shimadzu) in the region between 4000 and 1000 cm^{-1} with a spectral resolution of 1 cm^{-1} and an average of 25 scans.

Data analysis was performed using the multivariate data analysis software (SSPA 19.0, IBM, USA). A preprocessing of the FTIR spectra by the second derivative transformation and smoothing was given to separate overlapping absorption bands and remove the baseline offset. Multivariate statistical analysis technique of principal component analysis (PCA) was performed on the pretreated spectra. PCA involves the weighting of different factors and selection of principal components (PCs) that are used to classify groups of FTIR spectra into clusters based upon their degree of similarity. Each PC represents a factor of the spectrum. The factor PC1 represents the greatest variation in the spectra followed by PC2, which represents the second greatest variation and so on. PCA-based loading pilot analysis (LPA) can reflect the related chemical compositions which caused the clustering. It can help find the key variables and allows the wavenumbers responsible for the separation of the scores to be determined [18].

3. Results and discussion: The SEM image of the as-prepared AgNPs@AgCl grains is shown in Fig. 1*A*. It can be seen that disperse AgNPs were formed on the surface of the large AgCl grains. The size of the AgNPs was centred around 10–20 nm, except a few NPs with a diameter of about 60 nm, which may be caused by the particle agglomeration. The XRD patterns of the AgNPs@AgCl composite (Fig. 1*B*) exhibited diffraction peaks (2θ) at 27.8°, 32.2°, 46.2°, 54.8°, 74.5°, and 76.7°, which can be indexed to the (111), (200), (220), (311), (222), (400), and (420) plane reflections of AgCl (JCPDS Card No. 31-1238), respectively. In addition, a weak peak around 38.2° was present (Fig. 1*B*, inset), corresponding to the cubic phase of Ag (111) (JCPDS Card No. 65-2871). This result indicates that photoreduction is an efficient method for producing metallic Ag on the surface of AgCl grains.

The light absorption of the AgNPs@AgCl sample displayed a broad and strong absorption band in the range from visible (380 nm) to near infrared (>800 nm), as shown in Fig. 2 (the solid resulted in a great baseline). In addition, the maximal absorption appeared a flat plateau between 510 and 590 nm, which demonstrates the presence of the SPR of AgNPs with various diameters. Just because of its wide size distribution, the as-prepared AgNPs@AgCl composite could utilise the sunlight more efficiently.

The photocatalytic inhibition against the growth of *S. typhimurium* with the AgNPs@AgCl composite is shown in Fig. 3. In the dark controls (with the photocatalyst and without the light irradiation), the composite at concentrations of both 10 and 20 mg/l exhibited an insignificant influence on the bacterial growth, showing a similar trend to that of the blank (without the composite). The growth of *S. typhimurium* was weakly inhibited with 50 mg/l AgNPs@AgCl, and was obviously suppressed with 100 mg/l AgNPs@AgCl. While under the irradiation of visible light, the inhibition effect was clearly occurred with 10 mg/l AgNPs@AgCl and became more pronounced with the AgNPs@AgCl at higher concentrations. Using the composite of 20 and 50 mg/l, the bacterial cells were hardly grown up after half an hour. At the level of 100 mg/l, the growth of *S. typhimurium* was almost completely inhibited, and even the original bacteria were degraded as evidenced by that the OD_{600} value was lower than the beginning after 2 h.

The above results demonstrated the significant difference in the inhibition of the growth of *S. typhimurium* between the two processes using the AgNPs@AgCl composite under the dark condition and the visible light irradiation. It was verified that the inactivation of *S. typhimurium* is greatly enhanced by the photoreaction catalysed by the composite, which is due to the SPR of AgNPs. A mechanism as shown in Fig. 4 is suggested for the photocatalytic inactivation of bacterial cells. In detail, photons of visible light

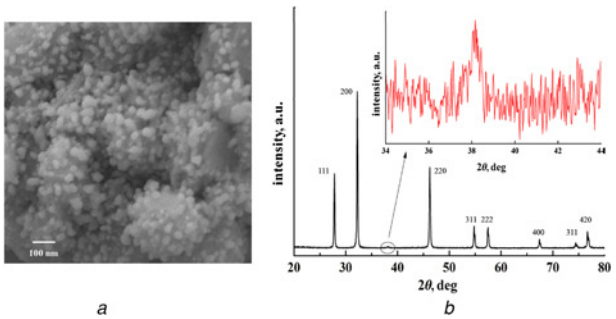

Fig. 1 *Characterisation of the AgNPs@AgCl composite*
a FESEM photograph
b XRD patterns

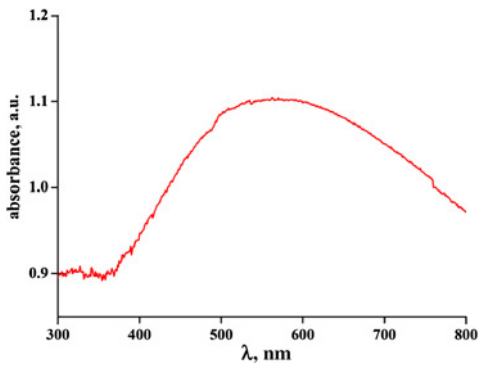

Fig. 2 *Absorption spectrum of the AgNPs@AgCl composite*

doi: 10.1049/mnl.2016.0560

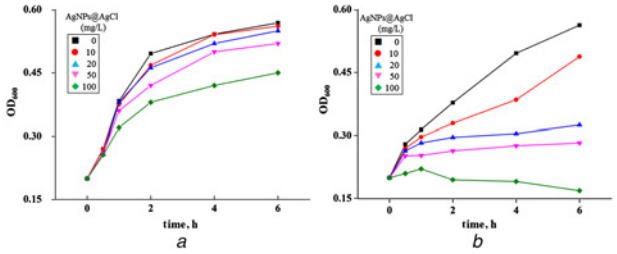

Fig. 3 *Growth curve of S. typhimurium in LB medium containing the AgNPs@AgCl composite at various concentrations*
a Dark
b Under the irradiation of visible light

are absorbed by AgNPs, generating pairs of electron–hole separated by the SPR-induced local electromagnetic field. Given that the surface of the AgCl grain is terminated by Cl^- ions and hence negatively charged, the electrons transfer to the surface of nanoparticles (NPs) farthest from the interface of AgNPs@AgCl, whereas the holes move to the AgCl surface. Subsequently, the photogenerated electrons are expected to be trapped by O_2 molecules in the solution to form ROSs such as $\bullet O_2^-$ radicals, meanwhile the holes react with the Cl^- ions to form Cl^0 atoms. Both ROSs and Cl^0 can oxidise bacterial biomolecules, making bacteria cells be injured or even death.

FTIR spectroscopy combined with chemometric analysis has been applied for studies of cellular compositions in *S. typhimurium* cells [19]. A typical FTIR spectrum of the *S. typhimurium* cells is shown in Fig. 5. The representative FTIR absorption bands were contributed from the molecular vibrations of functional groups, which constructed the basis of lipids, polysaccharides, DNA/RNA, and proteins of the microorganism cells. As shown in the figure, the strong and broad absorption band located in 3000–3600 cm^{-1} involves O–H stretch of water (ca. 3500 cm^{-1}) and N–H stretch of proteins (ca. 3200 cm^{-1}). The peak in the wavenumber from 3000 to 2800 cm^{-1} consists of C–H stretches by fatty acids in the cell wall and cell membrane. The peaks in the region of 1800–1500 cm^{-1} include C = O stretching (ca.1655–1637 cm^{-1}, amide I band) and N–H deformation (ca. 1550–1520 cm^{-1}, amide II band) of proteins, as well as the C = O stretching vibration of esters (ca. 1743 cm^{-1}). The peaks in the range from 1500 to 1200 cm^{-1} consist of C–H deforming of $>CH_2$ in phospholipids (ca.1470 cm^{-1}), C–H bending of $>CH_2$ in proteins (ca. 1448 cm^{-1}) and >C = O symmetric stretching of –COOH in proteins (ca. 1396 cm^{-1}), as well as P = O asymmetric and symmetric stretches of the phosphodiester backbones of DNA and RNA in nucleic acid (ca.1250–1220 cm^{-1}). Importantly, it can be seen from the figure that there was almost no difference in the FTIR spectra between the untreated and treated *S. typhimurium* cells. It is probably resulted from that the large cellular components in the bacterial cells could cause the spectral peaks be superimposed and broadened, leading to most of the information was hidden.

The second derivative conversion of the original infrared spectrum was generally able to separate the overlapping absorption bands. Meanwhile, the difference in spectra of bacteria with different treatments would be clearer with the help of chemometrics.

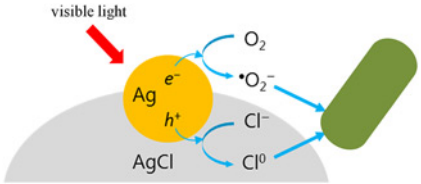

Fig. 4 *Schematics of photocatalytic inactivation of S. typhimurium with AgNPs@AgCl composite under VL irradiation*

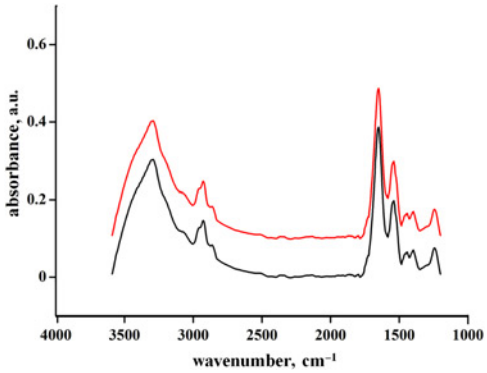

Fig. 5 *FTIR spectra of S. typhimurium cells photoinactivated with the AgNPs@AgCl composite (red: 0, black: 50 mg/l) after 2 h irradiation*

The result of PCA can display the similarity or the difference of the concentrated sample cube in the way of intuitive graphical data. The information of the second derivatively transformed FTIR spectra of *S. typhimurium* cells treated with the Ag@AgCl at various levels was extracted to carry out the PCA. The PCA in two spectral regions (1800–1500 and 1500–1200 cm^{-1}), which were selected based on the appearance of second-order peaks, are shown in Fig. 6. In these two spectral regions, the first two PCs accounted for over 85% of the total variance. It can be seen that the characters of bacterial cells in the absence of the Ag@AgCl were able to gather together into one narrow zone located on the left side of the first PC (PC1) and were obviously distinguished from the cells in the presence of the nanocomposite. On the right side of the PC1, a wide area was presented for the cells treated with the Ag@AgCl at the level of 100 mg/l. However, in the cases with the Ag@AgCl treatments at levels of 10–50 mg/l, the corresponding bacterial similarities were in transition regions between the above two extreme states. The distinction of these transition states required the combination of the first and the second PCs (PC1 and PC2). In a word, the bacterial cells photoinactivated with and without the Ag@AgCl can be completely separated, and the bacterial cells in different damage grades can also be isolated substantially. It should be noted that the centrifugation before the FTIR analysis used in the experiment might also cause some damages to the cells. Presented in the PCA results, these damages would be contributed to the similarity of the cells with the nanocomposite at the same level, but would be removed in the dissimilarities among the cells with the nanocomposite at different levels.

The first PC has a greater contribution to PCA regionalisation. The main absorption peaks in the loading plot of PC1 can be used to clarify the physiological changes of bacterial cells which were suffered from different treatments. There were ten absorption peaks (the loading value >0.1) in the case of *S. typhimurium*

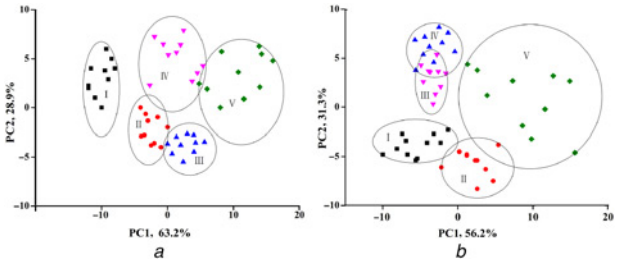

Fig. 6 *PCA obtained from the second derivative transformed FTIR spectra of S. typhimurium cells photoinactivated with the AgNPs@AgCl composite at different levels (I–V: 0, 10, 20, 50, 100 mg/l) after 2 h visible light irradiation*
a Spectral region: 1800–1500 cm^{-1}
b Spectral region: 1500–1200 cm^{-1}

photoinactivated with 100 mg/l AgNPs@AgCl. The peaks at 1693, 1674, 1650, and 1635 cm^{-1} belong to amide I, the peak at 1548 cm^{-1} is attributed by the characteristic band of amide II. They all belong to the bacterial proteins in the cell structure, indicating that the proteins of the bacterial structure were significantly changed by the photocatalytic treatment. The peaks at 1743, 1470, and 1396 cm^{-1} correspond to the vibrations of C=O stretching and C–H deformation of $>CH_2$ in lipids, as well as the C=O stretching in phospholipids, respectively. It suggests that the photoprocess using the composite induced destroying the lipids and phospholipids in the cell wall and membrane of *S. typhimurium*. The peak at 1240 cm^{-1} is attributed by DNA/RNA, implying the change in nucleic acids of the cells. Therefore, the proteins, nucleic acids, and lipids of *S. typhimurium* cells were changed, which means all the cell wall, cell membrane, and cytoplasm were damaged by the photocatalytic inactivation using the Ag@AgCl composite.

4. Conclusion: In summary, a composite consisting of AgNPs and AgCl grain (AgNPs@AgCl) was prepared and found to absorb light strongly and broadly in the region from visible to near infrared due to the SPR of the NPs. The AgNPs@AgCl composite was used to inactivate *S. typhimurium*, and it was found that the antimicrobial activity was significantly enhanced by the irradiation of the visible light. The photogenerated electrons and holes in the NP could produce reactive oxygen species and chlorine atoms, which degraded the structural proteins and lipids of the bacterial cells as revealed by the FTIR spectroscopy combined with chemometrics analysis. Finally, the preference of the photocatalytic killing to pathogens rather than normal cells is important in the food industry, particularly in regard to the raw food. From the results presented here, the photocatalytic inactivation using the nanocomposite might also cause damages to the healthy cells due to its destroying of the cell wall/membrane. Nevertheless, this material has potential applications for the cooked food. Moreover, the photocatalytic effect on the normal animal and plant cells will be addressed in the near future.

5. Acknowledgments: This work was supported by the Returned Overseas Chinese Scholars, State Education Ministry of China and the Chongqing Key Laboratory of Catalysis and Functional Organic Molecule (CQCM-2015-04).

6 References

[1] Crump J.A., Sjölund-Karlsson M., Gordon M.A., *ET AL.*: 'Epidemiology, clinical presentation, laboratory diagnosis, antimicrobial resistance, and antimicrobial management of invasive salmonella infections', *Clin. Microbiol. Rev.*, 2015, **28**, (4), pp. 901–937

[2] Ricke S.C., Donaldson J.R., Phillips C.A.: 'Food safety emerging issues, technologies and systems' (Academic Press, London, 2015)

[3] Maillard J.Y., Hartemann P.: 'Silver as an antimicrobial: facts and gaps in knowledge', *Crit. Rev. Microbiol.*, 2013, **39**, (4), pp. 373–383

[4] Marambio-Jones C., Hoek E.M.: 'A review of the antibacterial effects of silver nanomaterials and potential implications for human health and the environment', *J. Nanoparticles Res.*, 2010, **12**, (5), pp. 1531–1551

[5] Rai M.K., Deshmukh S.D., Ingle A.P., *ET AL.*: 'Silver nanoparticles: the powerful nanoweapon against multidrug – resistant bacteria', *J. Appl. Microbiol.*, 2012, **112**, (5), pp. 841–852

[6] Grigor'eva A., Saranina I., Tikunova N., *ET AL.*: 'Fine mechanisms of the interaction of silver nanoparticles with the cells of *Salmonella typhimurium* and *Staphylococcus aureus*', *BioMetals*, 2013, **26**, (3), pp. 479–488

[7] Rizzello L., Pompa P.P.: 'Nanosilver-based antibacterial drugs and devices: mechanisms, methodological drawbacks, and guidelines', *Chem. Soc. Rev.*, 2014, **43**, (5), pp. 1501–1518

[8] Le Ouay B., Stellacci F.: 'Antibacterial activity of silver nanoparticles: a surface science insight', *Nano Today*, 2015, **10**, (3), pp. 339–354

[9] Durán N., Durán M., de Jesus M.B., *ET AL.*: 'Silver nanoparticles: a new view on mechanistic aspects on antimicrobial activity', *Nanomedicine*, 2016, **12**, (3), pp. 789–799

[10] Elahifard M.R., Rahimnejad S., Haghighi S., *ET AL.*: 'Apatite-coated $Ag/AgBr/TiO_2$ visible-light photocatalyst for destruction of bacteria', *J. Am. Chem. Soc.*, 2007, **129**, (31), pp. 9552–9553

[11] Wang W., Huang G., Yu J.C., *ET AL.*: 'Advances in photocatalytic disinfection of bacteria: development of photocatalysts and mechanisms', *J. Environ. Sci.*, 2015, **34**, pp. 232–247

[12] McEvoy J.G., Zhang Z.: 'Antimicrobial and photocatalytic disinfection mechanisms in silver-modified photocatalysts under dark and light conditions', *J. Photochem. Photobiol. C*, 2014, **19**, pp. 62–75

[13] Wang P., Huang B., Qin X., *ET AL.*: '$Ag/AgBr/WO_{3\square}H_2O$: visible-light photocatalyst for bacteria destruction', *Inorg. Chem.*, 2009, **48**, (22), pp. 10697–10702

[14] Zhao L., Wang H., Huo K., *ET AL.*: 'Antibacterial nano-structured titania coating incorporated with silver nanoparticles', *Biomaterials*, 2011, **32**, (24), pp. 5706–5716

[15] Wang X., Lim T.-T.: 'Highly efficient and stable $Ag\text{-}AgBr/TiO_2$ composites for destruction of Escherichia coli under visible light irradiation', *Water Res.*, 2013, **47**, (12), pp. 4148–4158

[16] Kowalska E., Wei Z., Karabiyik B., *ET AL.*: 'Silver-modified titania with enhanced photocatalytic and antimicrobial properties under UV and visible light irradiation', *Catal. Today*, 2015, **252**, pp. 136–142

[17] Wang P., Huang B., Qin X., *ET AL.*: 'Ag@AgCl: A highly efficient and stable photocatalyst active under visible light', *Angew. Chem. Int. Ed.*, 2008, **47**, (41), pp. 7931–7933

[18] Lasch P., Naumann D.: 'Infrared spectroscopy in microbiology', *Encycl. Anal. Chem.*, 2015, pp. 1–32

[19] Sundaram J., Park B., Hinton A., *ET AL.*: 'Classification and structural analysis of live and dead Salmonella cells using Fourier transform infrared spectroscopy and principal component analysis', *J. Agric. Food Chem.*, 2012, **60**, (4), pp. 991–1004

doi: 10.1049/mnl.2016.0560